www.cadanda.com
Computer-Aided Design AND APPLICATIONS

The Promotion Effect of E-Learning in Intelligent Dance Teaching: Resource Mining Method on Dance Teaching

Xianli Li [1]
[1] Yunnan University of Finance and Economics, Kunming, Yunnan Province, China,650106,
Corresponding author: Xianli Li, 15887246550@163.com

Abstract. To improve the research effect of dance art, this paper focuses on the digital dynamic art of motion capture technology. Moreover, given the optimization problem in gesture estimation, this paper proposes an adaptive particle filter algorithm based on model intrinsic similarity for gesture estimation, which reasonably allocates computing resources and saves computing time. At the same time, this paper proposes a motion capture data retrieval method based on Laban symbols, which solves the problem of sample input in motion capture data retrieval and builds a dynamic art digital platform based on motion capture according to the actual needs of dance art research. In addition, through the parallel recording method of multi-view imaging technology, motion capture data, and motion spectrum recording, this paper designs experiments to verify the performance of the system constructed in this paper. The research results show that the system built in this paper has a specific effect.

Keywords: Digitization; image technology; gesture recognition; dance art; E-Learning.
DOI: https://doi.org/10.14733/cadaps.2024.S22.190-204

1 INTRODUCTION

The creation of a dance work is a process in which the choreographer expresses his feelings, cognition, appraisal, and desires of life through dance methods after being strongly infected in life. In this process, the choreographer chooses the subject matter of creation from the observation and experience of life. He shows his artistic thinking through artistic conception and specific and sensible artistic images. Suppose the selected image and the event to be expressed are difficult to induce the motivation of the dance and lack movement, and the plasticity of the dance is minimal. In that case, the possibility of sculpting sparkling dance art from this subject matter is minimal, so the artistic image created by the choreographer cannot be transmitted to the audience through dance [1].

Gesture and motion estimation are essential research directions in computer vision, which belong to the research field of middle vision. As a middle-level vision problem, gesture estimation uses low-level visual information, such as the contour, edge, and image blocon. At the same time, it provides a basis for analyzing and understanding the high-level semantic information of the target object's behavior. In the real world, most computer vision tasks are closely related to human activities, such as intelligent human-machine interfaces, health evaluation, and intelligent video surveillance. Visual analysis of human motion is an important research direction in computer vision. It aims to obtain human gesture and motion parameters by analyzing images or videos and conducting gesture recognition, semantic analysis, and behavior understanding [2].In the current research, the human body is usually modeled as a connected rigid body, so the research on the gesture estimation of the corresponding rigid body can provide meaningful guidance for estimating the human body gesture. The main research direction of this thesis is the gesture estimation of connecting the wooden body and the human body. At the same time, this thesis involves the research content of image segmentation, geometric vision, and pattern recognition [3].

Based on the above analysis, taking the dance art research of Yang Opera in Huaihua as an example, this paper combines digital gesture recognition technology to conduct dance art research.

The literature [4] has conducted a series of research on human tracking and detection. His research mainly uses the image structure to represent the two-dimensional human body gesture and dynamic programming to search for and solve the optimal gesture.

The literature [5] proposed an algorithm for 3D human tracking based on a simulated annealing particle filter, which has been cited nearly 700 times, and it has become one of the benchmark algorithms used in many researches on 3D human tracking or gesture estimation algorithms. The image features used in the algorithm proposed in the literature [6] are the foreground segmentation of the human body in the image sequence and the image edge information. Adding the simulated annealing step to the traditional particle filter algorithm [7]can prevent the search process from falling into the local minimum problem to a certain extent. The work of the literature [8] mainly focuses on estimating three-dimensional human body gestures. For the previous gesture estimation methods, such as the particle above filter-based algorithm, there are two main problems: initialization of the gesture and failure recovery. The three-dimensional human body gesture space contains the spatial position and rotation of the main parts of the human body. For commonly used models, it usually has 45-60 degrees of freedom [9]. The algorithm proposed in the literature [10] adopts a bottom-up idea, which believes that although the gesture of the entire human body is challenging to recover directly, the positioning of the partial body of the human body is a relatively simple problem. The literature [11] not only made excellent results in the gesture estimation algorithm but also provided researchers with an excellent body gesture database. By offering videos of a series of actions taken by a certain number of experimenters and the three-dimensional gesture truth values of the limbs given by the corresponding motion capture devices, the database will enable future researchers to obtain experimental data conveniently.

In the traffic system, for the pedestrian detection [12] or tracking [13] system, the human body is only treated as a rigid body occupying a particular spatial position and having a certain speed at this time. Therefore, it is only necessary to use a two-dimensional rectangle or a three-dimensional cylinder to describe. The Kinect [14], a human body real-time motion capture device launched by Microsoft for home TV entertainment, tracks 25 joint points in the whole body. Then, the three-dimensional space coordinates of these 25 key points constitute the gesture space of the virtual human body. Only part of the human body must be modeled for a gesture recognition system [15] or head tracking system [16]. In general, the gesture indicates that the determination of the space is closely related to the problem of concern.

The image feature space includes various features that express the human body in the image, such as contours, edges, and gradient histograms [17]. Gradient histogram has a certain degree of translation invariance, and it is robust in the presence of noise, so it has received extensive attention after its proposal [18].

2 TOPOLOGICAL CONSISTENCY MEASUREMENT OF DANCE ART

Disregarding the elastic deformation of human skin, the deformation of the human body model driven by human pose can be approximately described by isometric transformation. We assume the closest point pair is isometric in the manifold space when the human body model and shape are matched. In human motion capture based on multi-view images, due to human self-occlusion and other reasons, the reconstructed human shape contains noise, and even some limbs are connected, causing the topology of the human model to change. In this way, the geodesic distance cannot effectively describe the human posture deformation. The thermal diffusion distance based on Diffusion Geometry has isometric invariance and can effectively overcome the shortcomings of traditional local geometry affected by noise and attitude deformation.

The metric space is the most general and valuable topological space. First, we introduce the definition of rhythmic and metric space.

For the set X, it satisfies the function d with the following properties: $X \times X \to R$

1. For all $x, y \in X, d(x, y) \geq 0$, the equal sign is only valid when $x = y$;

2. For all $x, y \in X, d(x, y) = d(y, x)$;

3. For all $x, y, z \in X, d(x, y) + d(y, z) \geq d(x, z)$ (triangle inequality).

We call $d(x, y)$ a metric between x, y, and call (X, d) consisting of a set X and a metric d as a metric space.

The metric space has many valuable properties. The following mainly introduces the properties related to this paper.

1. Each metric space is a Hausdorff space.

2. We assume that (X, dX), and (Y, dY) are metric spaces. For a Bijection $f: X \to Y$, if there is $dX(x, x') = dY(f(x), f(x'))$ for every pair of points x, x' in X, then $f: X \to Y$ is said to be equidistant.If $f: X \to Y$ is equidistant, then the metric space X and Y are said to be equidistant.

3. We assume (X, dX), and (Y, dY) are metric spaces. According to the definition of an open set, the function $f: X \to Y$ is continuous. Only when there is an $\delta > 0$ for every $x \in X$ and any $\varepsilon > 0$ can there be $dY(f(x), f(x')) < \varepsilon$ when $x' \in X$ and $dX(x, x') < \delta$.

According to the nature of the metric space (2), we assume that when the human body model matches the shape of the human body, they are equidistant in the metric space $(X,)(\mathrm{dX})$ and Y, dY based on the thermal diffusion distance d. Therefore, we define a topological consistency metric based on thermal diffusion distance. The specific definition is:

$$D(X, Y) = \frac{1}{m} \sum_{p,q=1, p \neq q}^{m} \left(dX(x_p, x_q) - dY(y_p, y_q) \right)^2 \quad (1)$$

Laplace-Beltrami operator

Therefore, if f is a second-order differentiable objective function, the Laplacian operator of f is defined as:

$$\Delta f = \nabla^2 f = \nabla \cdot \nabla f \tag{2}$$

Among them, the Laplacian operator in the $x-y$ -dimensional plane is expressed in the Cartesian coordinate system as:

$$\Delta f = \frac{\partial^2 f}{\partial x^2} + \frac{\partial^2 f}{\partial y^2} \tag{3}$$

According to the definition of gradient and divergence on the Riemannian manifold, if g is the metric tensor on the manifold, the Laplace-Beltrami operator of the function f is expressed in the local coordinate system as:

$$\Delta f = \nabla \cdot \nabla f = \frac{1}{\sqrt{g}} \sum_{i,j=1}^{n} \frac{\partial}{\partial x_i} \left(\sqrt{|g|} g^{ij} \frac{\partial}{\partial x_i} f \right) \tag{4}$$

The main research object in computer graphics is digital geometry, a two-dimensional surface embedded in a three-dimensional Euclidean space. The discretization sampling technology is usually used to discretize the curved surface into a grid or point cloud to facilitate the representation and display. Therefore, discrete Laplace-Beltrami operators on triangular grids have also received more and more attention. When a function f is defined on a triangular mesh M with vertex n, the discrete Laplace-Beltrami operator $\Delta_M f(x_i)$ of the function at vertex x_i is defined as:

$$\Delta_M f(x_i) = \sum_{j=1}^{n} \omega_{ij} \left(f(x_i) - f(x_j) \right) \tag{5}$$

Among them, ω_{ij} is the weight constant, and Δ_M represents the second-order differential on the discrete grid M. The ideal Laplace-Beltrami operator should satisfy the following four conditions:

1. Symmetry: $\omega_{ij} = \omega_{ji}$;
2. Locality: if and only if vertex x_i is adjacent to vertex x_j, $\omega_{ij} \neq 0$;
3. Linear: For a linear function on the plane, there is $\Delta_M f(x_i) = 0$;
4. Non-negativity: when $i \neq j$, $\omega_{ij} \geq 0$.

Given the primary form of the discrete Laplace-Beltrami operator and the conditions that the coefficient ω_{ij} should satisfy, researchers have conducted much research on the value of ω_{ij}. Xu Guoliang and Fan Dian respectively summarized the specific calculation methods of the discrete Laplace-Beltrami operator, mainly including the Taubin discretization method, Desbrun discretization method, Mayer discretization method (based on the cotangent method), and so on. Since the discrete Laplace-Beltrami operator is the basis for effectively solving geometric partial differential equations, the convergence of the discrete Laplace-Beltrami operator is the primary issue. The definition of convergence is:

We assume that $M = \{M_i\}$ is a triangulation sequence of surface S and denote the set of vertices of M as X_j. If $x_i \subset x_{i+1}$, the triangulation sequence $\{M_i\}$ is said to be nested. We assume that the maximum side length of M_i is h_{M_i}, called the size of grid M_i. Then, we believe that $\{M_i\}$ is a nested triangulation sequence of a smooth surface S, and Δ_{M_i} is a discrete Laplace-Beltrami operator on M_i. At the same time, we assume that when $i \to \infty$, the grid size h_{M_i} tends to zero. If

$$\lim_{i \geq j, i \to \infty} \Delta_{M_i} x = \Delta_s x, \forall x \in X_j \tag{6}$$

then, the discrete Laplace-Beltrami operator Δ_{M_i} is said to be convergent.

The method based on cotangent in triangular meshes has gradually matured, and experiments have also proved that the discrete Laplace-Beltrami operator based on cotangent is convergent. The method based on cotangent as:

$$\Delta_M f(x_i) = \frac{1}{A(x_i)} \sum_{j \in N(i)} \frac{\cot \alpha_{ij} + \cot \beta_{ij}}{2} \left[f(x_i) - f(x_j) \right] \tag{7}$$

Among them, the angles α_{ij} and β_{ij} are the angles shown in Figure 1, $A(x_i)$ is the area of the Voronoi diagram area of vertex x_i (the sum of the areas of the triangles shown in Figure 2), and $N(i)$ is the set of adjacent points of vertex i. As shown in Figure 2, if the triangle $\Delta x_{j-1} x_i x_j$ is acute, then q_j is the outer center of the triangle. Still, if the triangle is obtuse, then q_j is the midpoint of the opposite side of the obtuse angle.

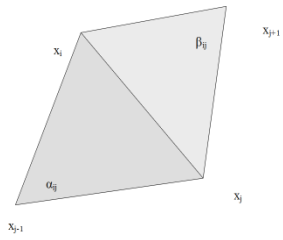

Figure 1: Definition of angles α_{ij} and β_{ij}.

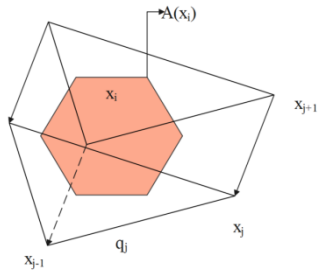

Figure 2: Definition of area $A(x_i)$.

For describing the discrete Laplace-Beltrami operator, the triangular mesh model is (GV, E), where v is the set of vertices of the triangular mesh, and E is the edges connecting the vertices. Then, the discrete Laplace-Beltrami operator can be represented by a matrix L, and the element L_{ij} of the Laplace matrix L is:

$$L_{ij} = \begin{cases} -\omega_{ij} & i \neq j \\ \sum k\omega_{ik} - \omega_{ij} & i = j \end{cases} \tag{8}$$

Among them,

$$\omega_{ij} = \begin{cases} \frac{\cot \alpha_{ij} + \cot \beta_{ij}}{2A(x_i)} & j \in N(i) \\ 0 & others \end{cases} \tag{9}$$

The thermal kernel function is based on the thermal diffusion theory on the Riemannian manifold, which uses the heat conduction equation (or heat equation) to describe the change of the heat distribution on the manifold over time. We assume that M is a complete n-dimensional smooth Riemannian manifold and believe that the heat equation is:

$$Lf(t) = \frac{-\partial f(t)}{\partial t} \tag{10}$$

Among them, L is the Laplace-Beltrami operator on the manifold M. $f(t)$ represents the heat distribution function at time t, and $f(0)$ is the heat distribution at the initial time. For a given heat distribution function $f(t)$, the fundamental solution of the equation is:

$$H(t) = e^{-tL} \tag{11}$$

We assume that $0 = \lambda_0 \le \lambda_1 \le \cdots \le \lambda_{n-1}$ is the eigenvalue of L, and the corresponding eigenvector is $\phi_0, \phi_1, \cdots, \phi_{n-1}$. Moreover, we set:

$$P_i = \phi_i^T \phi_i \tag{12}$$

Then,

$$L = \sum_{i=0}^{n-1} \lambda_i P_i \tag{13}$$

According to Taylor expansion $e^A = \sum_{k=0}^{\infty} \frac{A^k}{k!}$, there are:

$$H(t) = e^{-tL} = I - tL + \frac{t^2}{2!}L^2 - \frac{t^3}{3!}L^3 += I - t\sum_{i=0}^{n-1} \lambda_i P_i + \frac{t^2}{2!}\left(\sum_{i=0}^{n-1} \lambda_i P_i\right)^2 - \frac{t^3}{3!}\left(\sum_{i=0}^{n-1} \lambda_i P_i\right)^3 + \cdots \tag{14}$$

For

$$i \ne jP_iP_j = \phi_i^T\left(\phi_i\phi_j^T\right)\phi_j = 0P_iP_i = \phi_i^T\left(\phi_i\phi_i^T\right)\phi_i = \phi_i^T\phi_i \tag{15}$$

Therefore,

$$H(t) = I - t\sum_{i=0}^{n-1} \lambda_i P_i + \frac{t^2}{2!}\left(\sum_{i=0}^{n-1} \lambda_i^2 P_i\right)^2 - \frac{t^3}{3!}\left(\sum_{i=0}^{n-1} \lambda_i^3 P_i\right)^3 + \cdots = \sum_{i=0}^{n-1} e^{-\lambda_i t} P_i \tag{16}$$

Usually, the first K eigenvalues and eigenvectors that are not 0 are used in the calculation. Therefore, the element $h(p,q;t)$ of $H(t)$ is:

$$h(p,q;t) = \sum_{k=1}^{K} e^{-t\lambda_k}\phi_{p_k}\phi_{q_k} \tag{17}$$

The thermal diffusion distance of the two vertices in the triangular mesh is expressed as:

$$d_t^2(i,j) = h(i,i;t) + h(j,j;t) - 2h(i,j;t) = \sum_{k=1}^{K}\left(e^{-\frac{1}{2}t\lambda_k}\left(\phi_{ik} - \phi_{jk}\right)\right)^2 \tag{18}$$

Model-based methods usually regard the gesture estimation problem of multi-view images as an optimization problem. X is the human body model driven by the human body gesture parameter vector n, and y is the image's foreground (human body). The specific description is

$$\Phi = argmin\, D\left(Y, X(\Phi)\right) \tag{19}$$

The cost function design generally satisfies two requirements: one is that it must be able to reflect the matching degree of the gesture and the image foreground, and the other is that the computational complexity is as low as possible. The cost function proposed in this paper consists of three parts: contour matching metric, edge matching metric, and topology matching metric. The specific definitions are as follows:

$$D\big(Y,X(\Phi)\big)=\alpha_1 D_{Si1}\big(Y,X(\Phi)\big)+\alpha_2 D_{Edge}\big(Y,X(\Phi)\big)+\alpha_3 D_{Topo}\big(Y,X(\Phi)\big) \tag{20}$$

In contour matching and edge matching, the human body model is projected into the image, and the launched model satisfies the principle of small-hole imaging.

1. Contour matching items D_{Si1}

The contour of the human body is defined as the projection of the three-dimensional human body on the image plane, which can give the position information of the human body in space. At the same time, the contour still maintains a large amount of information reflecting the body's gesture estimation and understanding. The advantage of contouring is that it is not affected by skin tone, clothing, and lighting changes. The human body model X is projected onto the image plane to form a projection contour P, which matches the human contour S extracted from the image. The matching cost function is:

$$D_{Si1}\big(Y,X(\Phi)\big)=\sum_{i=1}^{n}\left(\begin{array}{l}\frac{1}{2|S_i^0|}\sum_{h\in S_i^0}|S_i(h)-P_i(h,\Phi)|\\+\frac{1}{2|P_i^0|}\sum_{h\in P_i^0}|S_i(h)-P_i(h,\Phi)|\end{array}\right) \tag{21}$$

Among them, $i=1\cdots,n$ is the camera number, h is the pixel number, S_i^0, P_i^0 is the set of pixels inside the contour and $|S_i^0|,|P_i^0|$ is the size of the set of pixels inside the contour. In contour matching, some pixels should be penalized when they are far from the contour, which can be achieved through Chamfer distance transformation. If distance transformation is performed on the projection profile P, then the distance transformation calculation must be completed for each projection, which significantly increases the amount of calculation. Therefore, only the human body contour S is generally subjected to distance conversion. In addition, a compromise can also be used to add a fixed value as a penalty to pixels that deviate from the contour.

2. Edge matching items D_{Edge}

In pose estimation, accurate edges can provide precise positions of human limbs. During model image matching, the edges of the dummy projected into the image plane are matched with the edges extracted from the image. There are many practical edge extraction algorithms to remove image edges, but the existing edge extraction algorithms mainly aim at the position of image grayscale or color mutation. This paper uses an edge detector based on a structured random forest. Figure 3 shows the result of edge detection. It can be seen from the figure that the extracted edge does not contain clothes texture and wrinkles [19].

The following describes the edge computing of the human body model. As shown in Figure 4, the projection of the human body model into the image for the point X on the skin surface; If the projection of point X in the image plane is located at the edge position, the following formula is satisfied:

$$n^T(X-C)=0 \tag{22}$$

Among them, C is the optical center coordinates of the camera. In actual calculations, the point cloud sampling points may only partially satisfy the above formula.

(a) (b) (c)

Figure 3: Edge extraction results based on structured random forest.

We set the threshold to $T(<0.1)$ and put the points helping $|n^T(X-C)|<T$ as the three-dimensional points corresponding to the edge of the image, and we project these points onto the image to form the limb projection edge. The projected edge contour and image edge of the human body model in the picture are obtained, and the similarity calculation formula is:

$$D_{Edge}=\sum_{i=1}^{n}\left(\begin{matrix}\frac{1}{|Se_i|}\sum_h d\left(Se_i,Pe_i(h)\right)\\+\frac{1}{|Pe_i|}\sum_h d\left(Se_i,Pe_i(h)\right)\end{matrix}\right) \tag{23}$$

Among them, $d\left(Se_i,Pe_i(h)\right)$ is the shortest distance from the projected contour point $Pe(h)$ to the edge Se of the image, calculated by Chamfer distance transformation. $i=1\cdots,n$ is the camera number, h is the pixel number, and $|Se|$ and $|Pe|$ represent the number of edge points [20].

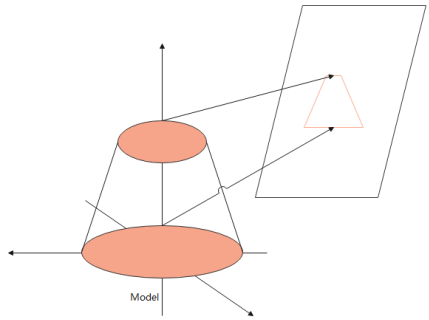

Figure 4: Limb edge model.

3. Topological consistency itemsD_{Topo}

The first two items measure the degree of matching between the human body shape and the human body model in the image plane. From the perspective of geometric attributes, they belong to the extrinsic distance measurement. In the three-dimensional space, when the model's gesture parameters perfectly express the human body's gesture, the human body model and the shape of the human body have topological consistency (isometric). Based on this assumption, the thermal diffusion distance of any point pair on the model should be similar to the thermal diffusion distance of the point pair formed by the closest point on the body shape. However, due to the presence of noise in the shape of the human body, the closest point pair does not satisfy the symmetry. We look

for the nearest point pair in both directions to reduce the influence of noise on the intrinsic distance. For the point set $P = \{p_1, \cdots, p_m\}$ on the human body model and the point set $Q = \{q_1, \cdots, q_n\}$ on the human body shape, $P' = \{p'_1, \cdots, p'_n\}$ and $Q' = \{q'_1, \cdots, q_m\}$ q' I m the closest point sets of the point set Q and P on the human body model and the human body shape. Thus, the topological consistency distance is defined as:

$$D_{Topo} = \sum_{i=1}^{n} \left\| \begin{pmatrix} D(P,P) & D(P,P') \\ D(P,P')^T & D(P',P') \end{pmatrix} - \begin{pmatrix} D(Q) & (Q,Q) \\ (,'Q'DQ,'QDQ,'Q)^T & D(Q,Q) \end{pmatrix} \right\| \tag{24}$$

The point sets P and Q are collected from the human body shape and the vertices of the human body model using the farthest distance sampling method.

The closest point pair of the human body shape and the human body model is searched through the KD-tree algorithm. It is necessary to calculate the eigenvalues and eigenvectors of the Laplacian matrix when calculating the thermal diffusion distance. If the eigenvalues and eigenvectors are calculated every time the model is deformed, the calculation amount is extensive and time-consuming. Generally, the skin deformation of the human body model driven by the predicted gesture vector is distance-preserving; that is, the skin deformation will not cause the topological structure of the human body model to change. Therefore, we only calculate the eigenvalues and eigenvectors of the Laplacian matrix corresponding to the T-Pose human body model during initialization and then directly substitute them in the subsequent calculations. In this way, each frame of gesture estimation only needs to calculate the eigenvalues and eigenvectors of the Laplacian matrix corresponding to the shape of the human body once. In this way, the increased amount of calculation is controllable, and the time-consuming is acceptable.

3 RESEARCH ON DANCE ART BASED ON DIGITAL GESTURE RECOGNITION

The above constructs the digital gesture recognition algorithm of this paper. With this algorithm's support, this paper researches dance art based on digital gesture recognition. Figure 5 shows the organizational structure of a dance art system based on digital gesture recognition, which mainly includes a data collection module, a data management module, and a multi-modal display module. The acquisition module is divided into three sub-modules: multi-view video acquisition module, motion capture data acquisition module (including logo motion capture system acquisition and non-identification motion capture system acquisition), and Laban motion spectrum automatic generation module based on motion capture data. The data management module mainly introduces two parts: metadata organization and data retrieval. The module includes a multi-view video display, a 3D human animation display, a Laban motion spectrum display, and a multi-mode simultaneous display [21].

The movement of the human body collected by the marked motion capture system mainly includes four steps: camera calibration, model initialization, motion capture, and output of motion capture data, as shown in Figure 6[22].

In this paper, a dance art system based on digital gesture recognition is constructed, and the system's performance is tested. Based on digital gesture recognition, this paper analyzes dance art movements. This article takes the study of the dance art of Yang Opera in Huaihua, Hunan, as an example for analysis. This article collects the dance of Yang Opera in Huaihua, Hunan, as the research object and sets up 100 sets of data to test the detection effect of digital gesture recognition. The results are shown in Table 1 and Figure 7.

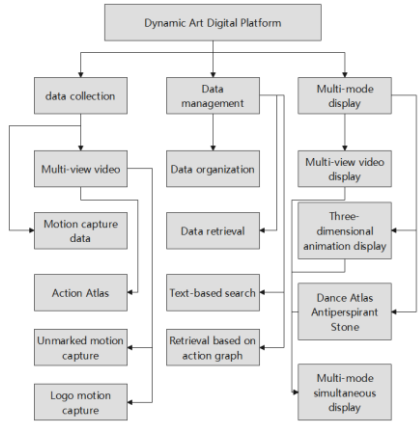

Figure 5: Dance art system based on digital gesture recognition.

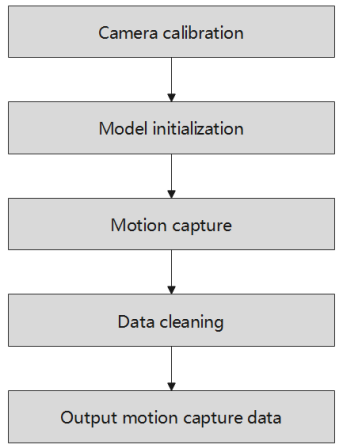

Figure 6: The operation process of the dance art gesture capture system.

Number	*Gesture recognition accuracy(%)*	*Number*	*Gesture recognition accuracy(%)*	*Number*	*Gesture recognition accuracy(%)*
1	*91.83*	*35*	*89.99*	*68*	*89.59*
2	*91.92*	*36*	*89.13*	*69*	*94.35*
3	*92.86*	*37*	*90.14*	*70*	*94.94*
4	*89.45*	*38*	*93.35*	*71*	*90.42*
5	*94.82*	*39*	*93.98*	*72*	*92.25*
6	*89.11*	*40*	*93.01*	*73*	*91.12*
7	*92.40*	*41*	*91.90*	*74*	*90.96*
8	*91.68*	*42*	*92.37*	*75*	*93.81*
9	*92.47*	*43*	*89.59*	*76*	*94.35*
10	*89.33*	*44*	*94.33*	*77*	*90.35*

11	92.49	45	90.38	78	90.91
12	92.70	46	89.86	79	89.79
13	92.40	47	91.83	80	89.58
14	91.54	48	89.53	81	94.39
15	94.74	49	93.20	82	92.77
16	93.71	50	91.94	83	89.05
17	90.38	51	93.06	84	91.99
18	89.70	52	90.90	85	90.16
19	92.13	53	94.47	86	91.50
20	91.12	54	90.62	87	91.16
21	92.38	55	94.97	88	89.50
22	93.79	56	94.85	89	91.74
23	90.34	57	89.15	90	90.33
24	92.43	58	90.70	91	93.60
25	90.64	59	90.10	92	91.14
26	94.38	60	92.77	93	92.43
27	94.04	61	93.81	94	93.67
28	89.57	62	93.37	95	94.71
29	92.76	63	90.52	96	93.79
30	93.67	64	92.89	97	89.34
31	93.24	65	91.22	98	93.08
32	93.81	66	92.85	99	91.47
33	93.58	67	91.93	100	94.70
34	89.28				

Table 1: Statistical table of the accuracy of digital gesture recognition.

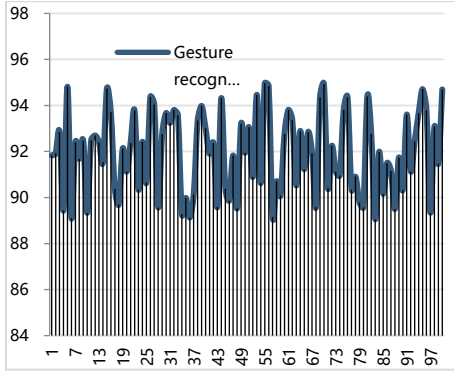

Figure 7: Statistical diagram of the accuracy of digital gesture recognition.

Through the above analysis, we can see that the dance art system based on digital gesture recognition constructed in this paper performs well in gesture recognition. Next, this paper evaluates

the art evaluation effect of the dance art system built in this paper on the analysis of dance art. The results are shown in Table 2 and Figure 8.

Number	*Performance evaluation score*	*Number*	*Performance evaluation score*	*Number*	*Performance evaluation score*
1	*83.90*	*35*	*84.69*	*68*	*84.96*
2	*90.62*	*36*	*84.28*	*69*	*85.91*
3	*84.19*	*37*	*89.39*	*70*	*87.27*
4	*90.41*	*38*	*83.29*	*71*	*90.44*
5	*84.66*	*39*	*84.16*	*72*	*86.70*
6	*87.34*	*40*	*84.38*	*73*	*85.61*
7	*86.53*	*41*	*84.73*	*74*	*83.96*
8	*86.31*	*42*	*89.42*	*75*	*88.26*
9	*89.43*	*43*	*87.29*	*76*	*89.21*
10	*85.79*	*44*	*90.81*	*77*	*88.59*
11	*87.87*	*45*	*88.18*	*78*	*85.55*
12	*89.64*	*46*	*83.82*	*79*	*84.65*
13	*88.53*	*47*	*86.39*	*80*	*90.44*
14	*90.65*	*48*	*83.17*	*81*	*90.51*
15	*83.95*	*49*	*90.01*	*82*	*88.38*
16	*90.81*	*50*	*84.71*	*83*	*83.35*
17	*83.93*	*51*	*87.43*	*84*	*88.04*
18	*86.13*	*52*	*84.06*	*85*	*84.95*
19	*86.10*	*53*	*87.25*	*86*	*86.26*
20	*84.77*	*54*	*84.29*	*87*	*88.76*
21	*86.97*	*55*	*87.03*	*88*	*83.17*
22	*85.43*	*56*	*85.50*	*89*	*89.45*
23	*86.90*	*57*	*90.54*	*90*	*83.77*
24	*86.33*	*58*	*84.11*	*91*	*89.61*
25	*86.51*	*59*	*86.43*	*92*	*89.51*
26	*86.10*	*60*	*87.72*	*93*	*87.80*
27	*85.48*	*61*	*88.08*	*94*	*88.58*
28	*88.29*	*62*	*90.80*	*95*	*89.09*
29	*87.37*	*63*	*89.12*	*96*	*86.25*
30	*87.35*	*64*	*90.68*	*97*	*83.75*
31	*88.48*	*65*	*88.11*	*98*	*85.68*
32	*88.36*	*66*	*85.33*	*99*	*90.65*
33	*85.50*	*67*	*84.16*	*100*	*88.93*
34	*88.12*				

Table 2: Statistical table of the art evaluation effect of the dance art system based on digital gesture recognition.

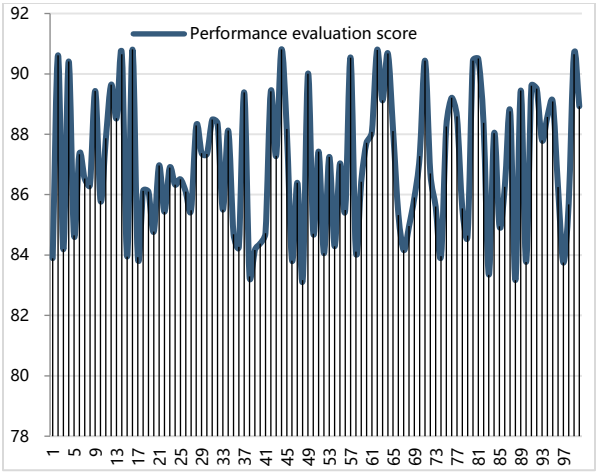

Figure 8: Statistical diagram of the art evaluation effect of the dance art system based on digital gesture recognition.

From the results of the above analysis, the dance art system based on digital gesture recognition constructed in this paper meets actual needs so that this system can be used in subsequent practice.

4 CONCLUSION

Our country has various dynamic arts, such as folk dances, opera figures, and Chinese martial arts, and the resources are extremely rich. Digital recording can prevent our country's vibrant art from being lost due to the death of the inheritor. Motion capture data is superior to video recording methods in motion representation, data reuse, and data management, and it can more effectively record and protect my country's dynamic art. This article combines digital gesture recognition technology to construct the dance art research system and combines the actual needs of dance analysis to build the model function module. Moreover, this paper designs experiments to analyze dance art, takes the dance art research of Yang Opera in Huaihua as an example, and combines digital gesture recognition technology to conduct dance art research. From the research results, the system constructed in this paper meets the expected requirements. The fusion of e-learning and intelligent resource mining will likely play an increasingly pivotal role in shaping the future of dance education.

Xianli Li, https://orcid.org/0009-0009-0087-3702

REFERENCE

[1] Fátima, S.; António, M.; Rocha, N. B. F.: et al. Kinematic parameters of throwing performance in patients with schizophrenia using a markerless motion capture system, Somatosensory Research, 32(2), 2015, 77-86. https://doi.org/10.3109/08990220.2014.969838

[2] Frost, D. M.; Beach, T. A. C.; Campbell, T. L.: et al. Can the Functional Movement Screen™ be used to capture changes in spine and knee motion control following 12 weeks of training? Physical Therapy in Sport, 23(6), 2016, 50-57. https://doi.org/10.1016/j.ptsp.2016.06.003

[3] Giannetti, R.; Petrella, A.; Bach, J.: et al. In vivo Bone Position Measurement Using High-Frequency Ultrasound Validated with 3-D Optical Motion Capture Systems: A Feasibility Study,

Journal of Medical & Biological Engineering, 37(7), 2017, 1-8. https://doi.org/10.1007/s40846-017-0273-x
[4] Holden, D.; Saito, J.; Komura, T.: A deep learning framework for character motion synthesis and editing, ACM Transactions on Graphics, 35(4), 2016, 1-11. https://doi.org/10.1145/2897824.2925975
[5] Juan, Pablo ngel-L.; Nelson, Arzola de la P.: Kinematic Hand Analysis Using Motion Capture Technology, IFMBE Proceedings, 49(6), 2015, 257-260. https://doi.org/10.1007/978-3-319-13117-7_67
[6] Khan, M. A.: Multiresolution coding of motion capture data for real-time multimedia applications, Multimedia Tools & Applications, 76(15), 2016, 1-16. https://doi.org/10.1007/s11042-016-3944-7
[7] Kim, M. K.; Kim, T. Y.; Lyou, J.: Performance Improvement of an AHRS for Motion Capture, Journal of Institute of Control, 21(12), 2015, 1167-1172. https://doi.org/10.5302/J.ICROS.2015.15.0116
[8] Komisar, V.; Novak, A. C.; Haycock, B.: A novel method for synchronizing motion capture with other data sources for millisecond-level precision, Gait & Posture, 51(3), 2016, 125-131. https://doi.org/10.1016/j.gaitpost.2016.10.002
[9] Lee, Y.; Yoo, H.: Low-Cost 3D Motion Capture System Using Passive Optical Markers and Monocular Vision, Optik International Journal for Light & Electron Optics, 130(2), 2016, 1397-1407. https://doi.org/10.1016/j.ijleo.2016.11.174
[10] Lin, C. H.: A Research on 3D Motion Database Management and Query System Based on Kinect, Lecture Notes in Electrical Engineering, 329(1), 2015, 29-35. https://doi.org/10.1007/978-94-017-9558-6_4
[11] Miura, T.; Kaiga, T.; Shibata, T.: et al. Low-dimensional Feature Vector Extraction from Motion Capture Data by Phase Plane Analysis, Journal of Information Processing, 25(6), 2017, 884-887. https://doi.org/10.2197/ipsjjip.25.884
[12] Park, S. W.; Park, H. S.; Kim, J. H.: et al. 3D displacement measurement model for health monitoring of structures using a motion capture system, Measurement, 59(5), 2015, 352–362. https://doi.org/10.1016/j.measurement.2014.09.063
[13] Puupponen, A.; Wainio, T.; Burger, B.: et al. Head movements in Finnish Sign Language based on Motion Capture data: A study of the form and function of nods, nodding, head thrusts, and head pulls, Sign Language & Linguistics, 18(1), 2015, 41-89. https://doi.org/10.1075/sll.18.1.02puu
[14] Rahman, M. M.: Analysis of Finger Movements of a Pianist Using Magnetic Motion Capture System with Six Dimensional Position Sensors, Transactions of the Virtual Reality Society of Japan, 15(3), 2017, C243-250.
[15] Shan, H.; Liu, Y.: Feature recognition of body dance motion in sports dancing, Metallurgical and Mining Industry, 7(7), 2015, 290-297.
[16] Wang, C. S.; Wang, L. H.; Kuo, L. C.: et al. Comparison of breast motion at different levels of support during physical activity, Journal of Human Sport and Exercise, 12(4), 2017, 1256-1264. https://doi.org/10.14198/jhse.2017.124.12
[17] Wang, S. K.; Xie, H.; Hu, B.: Research on Protection Property of Running Sportswear Fabrics Based on 3-D Motion Capture System, Textiles and Light Industrial Science and Technology, 3(2), 2014, 57-62. https://doi.org/10.14355/tlist.2014.03.009
[18] Xia, Q.; Zhang, M.; Gao, D. et al. Range of Hip Joint Motion and Weight of Lower Limb Function under 3D Dynamic Marker, Fa yixue za zhi, 33(6), 2017, 595-598.
[19] Zhang, A.; Yan, X. K.; Liu, A. G.: An Introduction to A Newly-developed Acupuncture Needle Manipulation Training-evaluation System Based on Optical Motion Capture Technique, Acupuncture Research, 41(6), 2016, 556-559.
[20] Zhang, H.; Wang, L.; Chu, S.: et al. Application of Optical Motion Capture Technology in Power Safety Entitative Simulation Training System, Optics & Photonics Journal, 06(8), 2016, 155-

163. https://doi.org/10.4236/opj.2016.68B026
[21] Zhou, L.; Bai, S.; Li, Y.: Energy Optimal Trajectories in Human Arm Motion Aiming for Assistive Robots, Modeling, Identification and Control (MIC), 38(1), 2017, 11-19. https://doi.org/10.4173/mic.2017.1.2
[22] Zhou, Z. M.; Chen, Z. W.: A Survey of Motion Capture Data Earning as High Dimensional Time Series, International Journal of Multimedia and Ubiquitous Engineering, 10(9), 2015, 17-30. https://doi.org/10.14257/ijmue.2015.10.9.03